Heliyon 9 (2023) e20189

Contents lists available at ScienceDirect

Heliyon

journal homepage: www.cell.com/heliyon

A two-stage SCUC model for distribution networks considering uncertainty and demand response

Fei Wang [a,*], Lei Gan [b], Pengchao Zhang [c]

[a] State Grid Hubei Jingmen Power Supply Company, Jingmen 448000, China
[b] State Grid Hubei Shiyan Power Supply Company, Shiyan, 442000, China
[c] State Grid Hubei Xiangyang Power Supply Company, Xiangyang, 441000, China

ARTICLE INFO

Keywords:
Demand response (DR)
Uncertainty
Component failure of power system
Marine predator algorithm

ABSTRACT

Demand response (DR) is one of the most effective and economical methods for power operators to improve network reliability in face of uncertainty and emergencies. In this paper, considering the uncertainty of wind power output and the failure of power system components, a two-stage security-constrained unit commitment (SCUC) model is established by optimizing the real-time pricing mechanism to indirectly adjust the DR. Firstly, the uncertainty of wind power output is modeled based on self-organizing map (SOM), and the component failure of the power system is modeled based on Monte Carlo. Then, a pricing scheme is proposed to stimulate users' electricity consumption behavior. Finally, the marine predator algorithm is used to solve the problem. Simulation results on IEEE-RTS system show that the proposed method can reduce the total operating cost by 10%, effectively stimulate the electricity consumption behavior of users, to improve the peak load shifting and valley filling capacity of the power system.

1. Introduction

Power system operation flexibility refers to the ability of the power system to respond to load demand changes on time and make it balanced [1]. With the further expansion of power grid-scale and the access to renewable energy, independent system operators will face greater challenges. Because of the unpredictability of network equipment accidents and the uncertainty of renewable energy output on the power supply side, the stability of power system operation is much hidden.

At present, the study of flexible operation of power system mainly focuses on the analysis of uncertain power output. Reference [2] studied the flexibility evaluation indicators and methods for multi-point distributed energy storage systems considering aggregation effects. Reference [3] established an optimization and regulation model for a fully renewable energy thermoelectric gas storage coupled energy supply system, addressing issues such as source, load uncertainty, and multi energy coupling. Reference [4] proposes a new model for allocating pumped storage hydroelectric units in Security-Constrained Unit Commitment (SCUC), taking into account the uncertainty of wind power plants. Reference [5] proposes a joint opportunity constrained unit commitment problem solving method based on improved risk allocation considering wind power uncertainty. Reference [6] incorporated the prediction error of wind power output into the mathematical model of unit combination through system rotation reserve, and designed a double-layer solution method. Reference [7] summarizes uncertainty management methods, parameter modeling, simulation tools, and testing systems in SCUC problems. Reference [8] proposes a distributed robust unit commitment model for N-k safety criteria under

* Corresponding author.
E-mail address: wfei37830@gmail.com (F. Wang).

https://doi.org/10.1016/j.heliyon.2023.e20189
Received 4 April 2023; Received in revised form 5 June 2023; Accepted 13 September 2023
Available online 26 September 2023

distributed uncertainty conditions. Reference [9] considers the uncertainty of wind power output and power equipment failures in the SCUC problem. Reference [10] proposes a scheme for solving adaptive robust SCUC problems using an online adjustment data-driven uncertainty set. Reference [11] proposes an unexpected robust unit commitment model. However, the above research still has two shortcomings: on the one hand, due to the influence of natural wind speed, the output of wind turbines is highly uncertain, making it difficult to directly establish accurate evaluation models; On the other hand, the above research on power system operation optimization considering the uncertainty of renewable energy output ignores the impact of the demand side.

Research shows that demand response (DR), as a basic element of future smart grid, cannot only reduce the impact of uncertainty of renewable energy output on the stable operation of power system, but also affect the power transaction price and improve the economy [12]. Literature [13] considered the comprehensive demand response and established a day ahead real-time two-stage risk economic optimization model of integrated energy system. Reference [14] established a power system scheduling model that considers wind power uncertainty and large user direct electricity purchases. Reference [15] proposes a distributed robust optimization method that calculates the risk of load shedding and renewable energy abandonment at the lower and upper bounds of the adjustable uncertainty set. Reference [16] comprehensively considers the penalty cost of wind abandonment, DR cost, and constraints of various units within the system to establish a scheduling model for the electric heating joint system. Reference [17] proposed a distributed economic dispatch model for interconnected AC/DC hybrid microgrids considering DR. Reference [18] proposed a multi microgrid collaborative optimization mechanism taking into account demand response. Literature [19] proposed a coordinated optimal dispatching model and method of integrated smart energy system considering the demand response of electric heating multi load. Literature [20] proposed a new real-time demand response market that cooperatively optimizes with the traditional energy market. Although the above research considers the impact of DR and improves the flexibility of power system operation, existing literature does not simultaneously consider the uncertainty risk of network component interruptions such as generator sets and transmission lines. Practical research has shown that DR is closely related to user electricity consumption behavior. In the power market, economic benefits are the main motivation for users to participate in grid fault recovery plans. If its impact is ignored, significant errors may occur when evaluating the flexibility of power system fault recovery.

In view of this, this article considers the uncertainty of wind power output and power system component failures, and indirectly adjusts DR by optimizing the real-time pricing mechanism. A two-stage SCUC model is established with the goal of minimizing operating costs. Firstly, starting from the historical data of wind turbine output, multiple high confidence feature output scenarios are calculated using the SOM clustering algorithm. By evaluating and calculating each scenario in the feature output scenario, uncertainty assessment of wind power output is achieved. Then, a pricing scheme was proposed to incentivize users' electricity consumption behavior, and an SCUC model considering uncertainty and DR was established. Finally, the ocean predator algorithm is used to solve the problem. The effectiveness of the proposed method was verified through simulation examples based on the IEEE-RTS system.

Main contributions of this paper.

1. Demand-side response factor was added in the SCUC modeling solution process considering the uncertainty of renewable energy output.
2. While considering the influence of DR, the uncertain risks caused by the interruption of generator sets and transmission lines are also considered.
3. Marine predator algorithm was introduced to solve the uncertain SCUC model.

2. Evaluation of uncertain variables

The SCUC model studied in this paper considers two types of uncertain variables: the uncertainty of wind power output and the uncertainty of system component failure. Wind power output is a continuous variable, while system component failure is a discrete variable (take 0 and 1). Therefore, this section establishes evaluation models for two different types of uncertain variables.

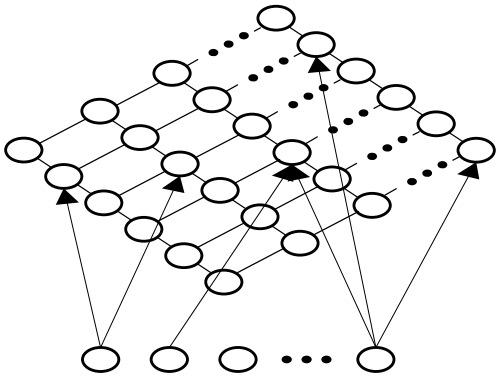

Fig. 1. The structure of SOM.

2.1. Uncertainty assessment of wind power output

Self-organizing map (SOM) is a kind of neural network, which is suitable for unsupervised clustering of data [21]. SOM has only input layer and output layer. As shown in Fig. 1. The input layer inputs the historical data of wind power output to be clustered, and the output layer outputs the clustering results.

The training process of the SOM network is to find the output layer unit with the shortest distance and update it based on the input data. A node in the output layer represents the class that is finally aggregated. The clustering steps are shown in Fig. 2.

2.2. Uncertainty assessment of system component failures

Failure of power system components is usually difficult to predict directly and this kind of failure will almost always result in outage of generator sets and transmission lines. This section uses the statistical analysis method of historical data to model the failure probability of generator set outage and transmission line outage. Firstly, the failure frequency of each type of system component is obtained through massive historical data analysis, which is regarded as the probability of failure. Then a certain number of random scenes are obtained based on Monte Carlo simulation method. The evaluation steps are shown in Fig. 3.

3. SCUC model considering uncertainty and demand response

The SCUC model studied in this paper considers the uncertainty of wind power output, uncertainty risk and DR. In the first stage, the system day-ahead SCUC decision is modeled and solved. In the second stage, considering the uncertainty of wind power output and system component failure, the first stage's decision results are adjusted. DR is considered in both models. The initial demand profile, power user elasticity data and their participation rate are all known input data. In addition, generator parameters, power transmission line data and network basic data are known data. The decision-making variables of the model are the load of each node, the real-time electricity price of each node, the optimal scheduling scheme of unit output, load reduction and operation cost.

3.1. Demand response model and constraints

Demand price elasticity matrix is one of the more practical methods in DR modeling, which can effectively evaluate consumers'

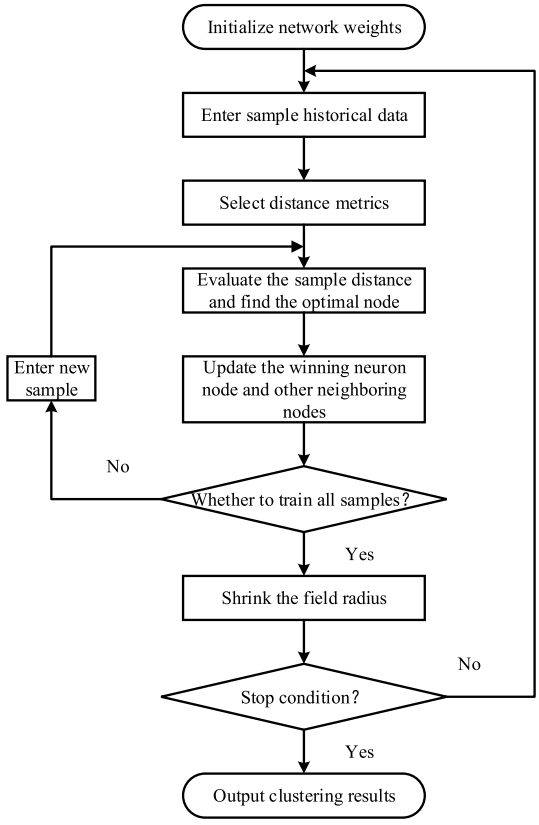

Fig. 2. The Steps for SOM clustering method.

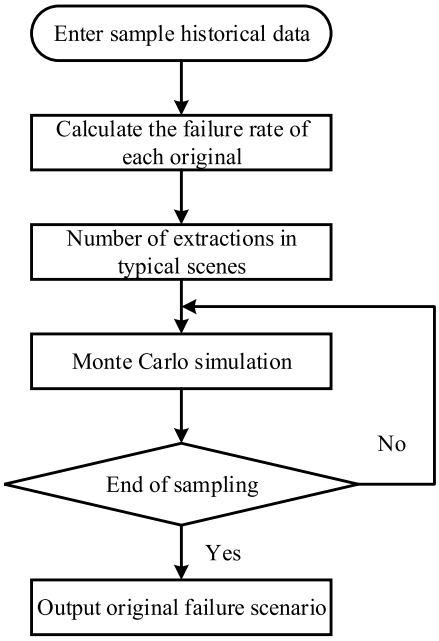

Fig. 3. The Steps for system component failure.

behavior preferences. In this model, the elasticity of electricity demand $E_{tt'}$ is described as the price deviation of the demand change at the $t^{'}$ th moment relative to the t h moment, as shown in equation (1).

$$E_{tt'} = \frac{\partial q_t}{q_t} \cdot \frac{\rho_{t'}}{\partial \rho_{t'}} \tag{1}$$

Where ∂q_t and $\partial \rho_{t'}$ are the changes of user's electricity demand and t 'time price respectively. q_t and $\rho_{t'}$'are the benchmark values of the electricity demand and the electricity price at t' time respectively. When $t = t'$, $E_{tt'}$ is called self-elastic coefficient; when $t \neq t'$, $E_{tt'}$ is called mutual elastic coefficient.

The relationship between electricity demand and electricity price is shown in equation (2) [22].

$$q_t = q_t^0 \cdot \left[1 + \frac{\sum_{t'=1}^{T} E_{tt'} \cdot \left(\rho_{t'} - \rho_t^0 \right)}{\rho_t^0} \right] \tag{2}$$

Where T is the dispatching period, ρ_t^0 is the initial value of t t' time price, q_t^0 is the initial value of user's power demand at t moment.

In order to limit the rationality of the pricing scheme, we need to consider the actual constraints. In order to maximize the potential of fault recovery and the DR capability of power users, this paper assumes that the minimum price is achieved in the case of minimum demand, and the maximum price is achieved in the case of maximum demand. By changing the real-time price, it can effectively motivate the power users to transfer the transferable load to the low load period, which means it can improve the power users' ability to cut peak and fill valley through the price.

1) Upper and lower limit constraints of peak load shifting of user

$$-q^{max} \leq \triangle q_t \leq q^{max} \tag{3}$$

Where q^{max} refers to the upper limit of the load demand for peak load shifting acceptable by power users. Δq_t is the increment of peak load shifting at t time, when $\Delta q_t > 0$, it means the load increases, and when $\Delta q_t < 0$, it means the load is reduced.

2) Total demand constraints of power users

$$\sum_{t=1}^{T} \triangle q_t = 0 \tag{4}$$

Equation (4) shows that the total power demand of each node remains unchanged during the implementation of DR strategy. This means the load is transferred from peak period to low load or non-peak period.

3.2. Two-stage SCUC model

In this section, a two-stage SCUC model considering uncertainty and Dr is established. In the first stage, the mathematical model is established to minimize the operation cost, start-up cost and spinning reserve cost of thermal power units without considering the uncertainty. In the second stage, considering the uncertainty, the mathematical model is established to minimize the power purchase cost and wind abandonment cost of wind turbines, reduce the load cost and adjusting the spinning reserve cost of thermal power units in the first stage. The models for each stage are as follows.

3.2.1. First stage model

The mathematical model of SCUC established in the first stage is as follows.

(1) First stage objective function

$$\boldsymbol{min}\ C_1 = \sum_{t=1}^{T}\sum_{i=1}^{G}\begin{bmatrix}\left(a_i + b_i P_{Git} + c_i {P_{Git}}^2\right)\cdot I_{Git}\\ +I_{Git}\cdot\left(1 - I_{Gi(t-1)}\right)\cdot C_{Gi}^{UD}\\ +\left(C_{Git}^{U}\cdot P_{Git}^{U} + C_{Git}^{D}\cdot P_{Git}^{D}\right)\end{bmatrix} \tag{5}$$

Where: T is the scheduling period; t is the scheduling time; G is the number of thermal power units that can be scheduled. i is the ith schedulable thermal power unit, a_i、 b_i and b_i are the generation cost coefficients of thermal power units. P_{Git} is the active power output of the ith thermal power unit at time t， I_{Git} is the binary variable of the operation state of the ith thermal power unit at time t, 1 means start-up operation, and 0 means shutdown. C_{Ci}^{UD} represents the start-up and shutdown costs of the first thermal power unit. To simplify the model, only the start-up costs are considered, and the shutdown costs are ignored. P_{Git}^{U} and P_{Git}^{D} represent the active power positive and negative rotation reserve of the first thermal power unit a t time t, respectively. C_{Git}^{U} and C_{Git}^{D} represent the positive and negative spinning reserve costs per unit active power of the ith thermal power unit a t time t, respectively.

(2) Stage 1 Constraints

1) Output Limitation Constraints for Thermal Power Units

$$I_{Git}\cdot P_{Gi}^{min} \le P_{Git} \le I_{Git}\cdot P_{Gi}^{max} \tag{6}$$

Where: P_{Gi}^{min} and P_{Gi}^{max} are the lower limit and upper limit of the active power output of the ith thermal power unit at time t respectively.

2) Restriction of start-stop times of thermal power units

$$\sum_{t=1}^{T}\left|I_{Git} - I_{Gi(t-1)}\right| \le N_i \tag{7}$$

Where: N_i is the maximum allowable number of start and stop times of the ith thermal power unit in the dispatching period.

3) Minimum start-stop time constraint

$$\sum_{\tau=t+2}^{t+MUT_{Gi}}\left(1 - I_{Gi\tau}\right) + MUT_{Gi}\left(I_{Gi\tau} - I_{Gi(\tau-1)}\right) \le MUT_{Gi} \tag{8}$$

$$\sum_{\tau=t+2}^{t+MDT_{Gi}} I_{Gi\tau} + MDT_{Gi}\left(I_{Gi(\tau-1)} - I_{Gi\tau}\right) \le MDT_{Gi} \tag{9}$$

Where: MUT_{Gi} and MDT_{Gi} represent the minimum start-up time and minimum shutdown time of the ith thermal power unit respectively.

4) Landslide restraint of thermal power units

$$\sum_{i=1}^{G}\left[\Delta P_{Gi}^{U} I_{Git} + P_{Gi}^{min}\left(I_{Git} - I_{Gi(t-1)}\right)\right] \ge \sum_{i=1}^{G} P_{Git} - P_{Gi(t-1)} \tag{10}$$

$$\sum_{i=1}^{G}\left[\Delta P_{Gi}^{D} I_{Gi(t-1)} + P_{Gi}^{min}\left(I_{Gi(t-1)} - I_{Git}\right)\right] \ge \sum_{i=1}^{G} P_{Gi(t-1)} - P_{Git} \tag{11}$$

$$-\Delta P_{Gi}^{D} \le P_{Git} - P_{Gi(t-1)} \le \Delta P_{Gi}^{U} \tag{12}$$

Where ΔP_{Gi}^{U} and ΔP_{Gi}^{D} are the maximum climbing and sliding rates of the active power output of the i-th thermal power unit per hour.

5) Reserve capacity constraint

$$P_{Git} + P_{Git}^{U} \le P_{Gi}^{max} \cdot I_{Git} \tag{13}$$

$$P_{Git} - P_{Git}^{D} \ge P_{Gi}^{min} \cdot I_{Git} \tag{14}$$

$$0 \le P_{Git}^{U} \le \Delta P_{Gi}^{U} \cdot \Psi_i \tag{15}$$

$$0 \le P_{Git}^{D} \le \Delta P_{Gi}^{D} \cdot \Psi_i \tag{16}$$

Where Ψ_i refers to the time required for the i-th thermal power unit to turn its rotating reserve into formal output.

6) Wind turbine output constraints

$$0 \le P_{Wwt} \le P_{Ww}^{max} \tag{17}$$

Where: W is the number of schedulable wind turbines, w is the w-th schedulable wind turbine, P_{Wwt} is the active power output of the ith wind turbine at time t, P_{Ww}^{max} is the upper limit of the active power output of the wth wind turbine.

7) Incremental load demand constraints

$$\Delta q_t = q_t - q_{t-1} \tag{18}$$

8) Power balance constraints

$$\sum_{i=1}^{G} P_{Git} + \sum_{w=1}^{W} P_{Wwt} = q_t \tag{19}$$

9) Network power flow constraints

$$P_l = \sum_{i=1}^{G} (K_{Gli} \cdot P_{Git}) + \sum_{w=1}^{W} (K_{Wlw} \cdot P_{Wwt}) - \sum_{b=1}^{B} (K_{Blb} \cdot q_{bt}) \tag{20}$$

$$P_l = \frac{\theta_m - \theta_n}{X_{mn}} \tag{21}$$

Where, K_{Gli}, K_{Wlj} and K_{Dlk} represent the network transfer factors of thermal power units, wind turbines and load demand respectively. B is the total number of load demand nodes; b is the number of load nodes. m and n are the numbers of the first and end of the first line; θ_m and θ_n are the voltage phase angle of the first and end of the first line. X_{mn} is the reactance of the first line; P_l is the active power flowing through the *l-th line*.

10) Line safety constraints

$$-P_l^{max} \le P_l \le P_l^{max} \tag{22}$$

Where P_l^{max} is the upper limit of the absolute value of active power flowing through line l.

3.2.2. Second stage model

(1) Second stage objective function

$$\boldsymbol{min}\ C_2 = \sum_{s=1}^{S}\gamma_s\left\{\sum_{t=1}^{T}\left[\begin{array}{l}\sum_{i=1}^{G}\left(C_{Gits}^{U}\cdot P_{Gits}^{Ure}+C_{Gits}^{D}\cdot P_{Gits}^{Dre}\right)\\ +\sum_{w=1}^{W}\left(C_{Wwts}\cdot P_{Wwts}+C_{Wwts}^{cut}\cdot P_{Wwts}^{cut}\right)\\ +\sum_{b=1}^{B}\left(C_{Gbts}^{\Delta}\cdot|\Delta q_{bts}|\right)\end{array}\right]\right\} \tag{23}$$

In this equation, s represents the set of uncertain scenes; s represents the s-th uncertainty scene. γ_s is the probability of scene s. P_{Gits}^{Ure} and P_{Gits}^{Dre} represents the positive and negative spinning reserve of the i-th thermal power unit's active power at time t under the s-th uncertainty scenario. C_{Gits}^{U} and C_{Gits}^{D} represent the positive and negative spinning reserve costs of the i-th thermal power unit's active power at time t under the s-th uncertainty scenario. P_{Wwts} is the active power output of the ith wind turbine at time t under the s-th uncertainty scenario, P_{Wwts}^{cut} is the abandoned wind power of the ith wind turbine at time t under the s-th uncertainty scenario. C_{Wwts} is the price of purchasing power from the i-th wind turbine at time t under the s-th uncertainty scenario. C_{Wwts}^{cut} is the wind abandonment cost of the i-th wind turbine at time t under the s-th uncertainty scenario. C_{Gbts}^{Δ} is the cost of load demand transfer (peak load shifting) connected with node *b* at time t under the s-th uncertainty scenario. Δq_{bts} is the increment of load demand connected with node b at time t in the s-th uncertain scenario.

(2) Second stage constraints

1) Network power flow constraints in uncertain scenarios

$$\omega_{ls}\cdot P_{ls} = \sum_{i=1}^{G}\left(\lambda_{Gits}\cdot K_{Gli}\cdot P_{Gits}\right)+\sum_{w=1}^{W}\left[K_{Wlw}\cdot\left(P_{Wwts}-P_{Wwts}^{cut}\right)\right]-\sum_{b=1}^{B}\left(K_{Blb}\cdot q_{bt}\right) \tag{24}$$

Where λ_{Gits} is the binary variable of fault indication of the ith thermal power unit at time t under the s-th uncertainty scenario. ω_{ls} is the binary variable of fault indication of the 1st line under the s-th uncertainty scenario. 1 is normal operation and 0 is fault shutdown.

2) Wind turbine curtailment constraints

$$0 \le P_{Wwts}^{cut} \le P_{Wwts} \tag{25}$$

3) Reserve capacity constraints in uncertain scenarios

$$0 \le P_{Gits}^{Ure} \le P_{Gits}^{U} \tag{26}$$

$$0 \le P_{Gits}^{Dre} \le P_{Gits}^{D} \tag{27}$$

4. 4.solving method of SCUC model based on MPA

Marine predator algorithm (MPA) is an efficient intelligent search algorithm, which takes the foraging behavior of fish in the ocean as the basic idea. The foraging technique of MPA depends on two random motion processes: Levy flight motion and Brownian motion. Research shows that when MPa is looking for food, it takes Levy flight as its motion mode, and when it is chasing food, its motion mode is converted to Brownian motion [23]. In addition, the fish aggregation device (FAD) describes another behavior related to the movement of predators such as sharks, that is, the predator suddenly jumps vertically. The steps of MPA algorithm are as follows.

Step 1. initialization

The random initialization of MPA population is as follows

$$X_i = X_i^{min} + \left(X_i^{max} - X_i^{min}\right)\times rand \tag{28}$$

$$X = \begin{bmatrix} X_{11} & X_{12} & \cdots & X_{1v} \\ X_{21} & X_{21} & \cdots & X_{2v} \\ \vdots & \vdots & \cdots & \vdots \\ X_{u1} & X_{u1} & \cdots & X_{uv} \end{bmatrix}_{u\times v} \tag{29}$$

Where X_i^{max} and X_i^{min} represent the maximum and minimum values of the ith predator respectively. X_i represents the variable to be solved of the ith predator. *Rand* represents the uniform random number in the generation interval [0,1]. X represents the population matrix composed of multiple marine predators; u *and v* represent the total number of marine predators and the number of variables to be solved respectively.

Step 2. Levy motion and Brownian motion of MPA

In this step, according to the speed ratio between predator and prey, it is divided into three stages, and the positions of predator and prey are updated in each stage.

1) The speed of the predator is higher than that of the prey. In this stage, the position of predator and prey is updated by Brownian motion

$$SZ_i = R_{Br} \times (E_i - R_{Br} \times X_i) \tag{30}$$

$$X_i^{'} = X_i + \frac{1}{2} \cdot R \times SZ_i \tag{31}$$

Where, R_{Br} is the vector-based on Brownian motion representation. E_i is the optimal location matrix of the MPA population S Z_i is the predator moving step vector. $_{\mathrm{R}}$ is the uniform random vector. $X_i^{'}$ is the updated MPa population location matrix. $\times$ is the vector or matrix multiplication.

2) The speed of the predator is lower than that of the prey. In this stage, the position of predator and prey is updated by levy motion. The levy motion model is as follows:

$$SZ_i = R_{Le} \times (R_{Le} \times E_i - X_i) \tag{32}$$

$$X_i^{'} = E_i + \frac{1}{2} \cdot R \times SZ_i \tag{33}$$

Where R_{Le} is the vector-based on levy motion representation.

3) The speed of the predator is equal to that of the prey. At this stage, the MPA population is divided into two groups. One group was looking for food; the other group was chasing food. The positions of predator and prey are updated by Levy flight motion and Brownian motion, as shown in 1) and 2) respectively.

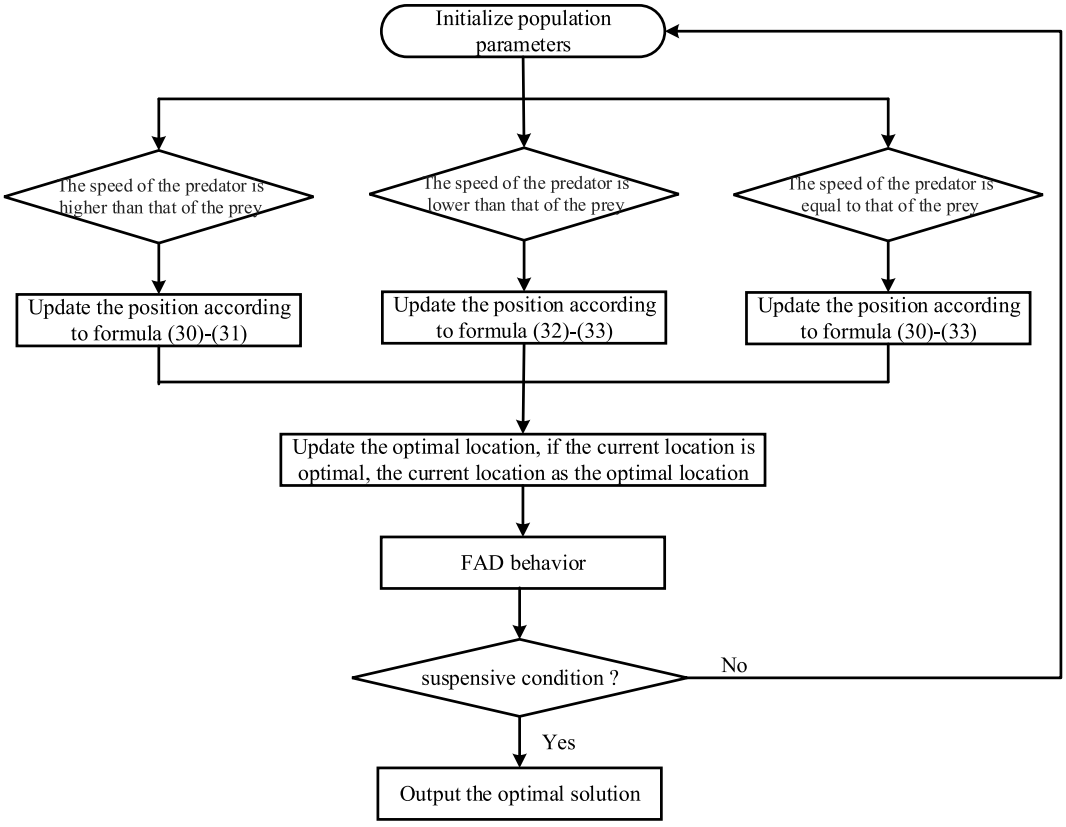

Fig. 4. Flowchart of MPA algorithm.

Step 3. Fad behavior

As described in step 2, there are only three kinds of normal predator-prey behaviors, and the existence of FAD behavior may make the algorithm itself fall into local optimum. Therefore, it is necessary to model FAD behavior and obtain local optimal solution. The fad model is as follows:

$$X_i^{'} = \begin{cases} X_i + C_F \cdot \left[X_i^{min} + R_{Le} \times \left(X_i^{max} - X_i^{min}\right)\right] \times rand & r \le \xi_{FAD} \\ X_i + \left[\xi_{FAD} \cdot (1-r) + r\right] \cdot (X_{r1} - X_{r2}) & r \succ \xi_{FAD} \end{cases} \tag{34}$$

Where C_F is the adaptive parameter controlling the predator's moving step; ξ_{FAD} is the probability of fad behavior; r1 and r2 are the random indexes in the prey matrix.

The detailed step flow chart of solving the SCUC model based on MPA is shown in Fig. 4.

5. Example analysis

This paper takes the IEEE-RTS system as the basis for the analysis of simulation examples. The system consists of 24 nodes and 38 lines. The thermal power group is connected to nodes 1, 2, 7, 13, 16, 18, 21, 22, 23, 24, respectively. Wind turbines are connected to Nodes 2 and 21, respectively. The connection of the IEEE-RTS system is shown in Fig. 5.

The load data used in this section is the actual load data of a region reduced by a certain ratio year-on-year, with a total load of 2670 MWh.In the same way as the load data is processed, the output history data of multiple wind turbines collected in an area is transformed with the same scale as the source of the simulation data in this paper. Considering the increasing proportion of renewable energy in the actual power system, this paper sets the total power generation of wind turbines to 30% of the total power generation, which is 1200 MW. The elastic matrix of user demand for electricity is obtained by the method of reference [22]. The price of electricity purchased from wind turbines is 20$/MWh and the cost per unit capacity of wind power reduction is 35$/MWh. The reason why the cost per unit capacity of wind power reduction is higher than the electricity purchase price is to encourage clean energy to enter the network and reduce environmental pollution. According to the SOM method in Chapter 1, wind power is clustered, and three groups of wind power data of typical types are obtained, namely, three uncertain scenarios of wind power in this paper. Scheduling cycle T = 24 h. Related calculations are based on MATLAB 9.0 programming, computer environment is Intel Core i7-7700, 16G.

To assess the effectiveness of this model, this papr is divided into four cases.

Case 1. Fixed electricity price considering the uncertainty of wind power.

Case 2. Consider the uncertainty of wind power and the interaction between real-time electricity price and DR.

Case 3. Consider the uncertainty of wind power, fixed electricity price, and power system component failure.

Case 4. Consider the uncertainty of wind power, the interaction between real-time electricity price and DR, and the failure of power

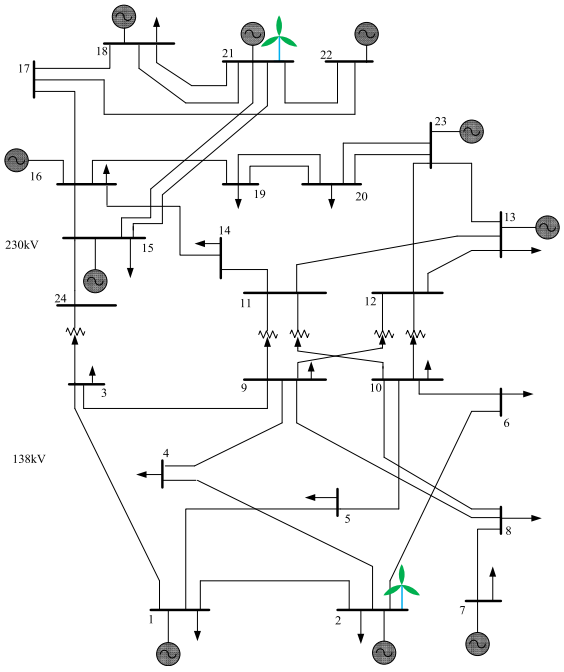

Fig. 5. The system diagram of IEEE-RTS.

system components.

5.1. Case 1 simulation result analysis

In case one, it is to decide on SCUC considering the uncertainty of wind power output under the fixed electricity price scheme [24, 25]. The total operating cost of SCUC and the total user electricity cost obtained by the third chapter solution method are 749334$ and 122 6616$, respectively. The cost of electricity purchase is calculated by multiplying the fixed electricity price by the total power purchased per hour. Involuntary wind abandonment due to impractical wind power generation plans and excessive wind generation accounted for 0.088% (2.35 MWh) and 0.32% (8.63 MWh) of total power demand, respectively.

5.2. Case 2 simulation result analysis

Case two considers the interaction between real-time electricity price and DR, and also considers the uncertainty of wind power output to make SCUC decisions. This section sets 10% of the total electricity users to participate in DR interaction. Table 1 shows the real-time electricity price in Case 2.

First, assume that all power users participating in the DR interaction are short-term power consumers. This means in the current period of time, power demand changes based on real-time price changes. Therefore, its demand-price elastic matrix contains only diagonal elements, i.e., which is the self-elastic coefficient. The calculated total operating cost and the total user purchase cost are 745236$and 102099$, respectively. Compared with the case one result, the total operating cost is reduced by 1%, and the total user purchase cost is 10%. Involuntary wind abandonment due to impractical wind generation plans and excessive wind power generation accounted for 0.076% (2.05 MWh) and 0.23% (6.21 MWh) of total power demand, respectively. Compared with case one, the interaction between real-time electricity price and DR can significantly reduce the operating and purchasing costs of power systems, which proves the applicability of DR in improving the flexibility of power systems.

However, not all electricity users are short-term consumers. Some users may change their demand for electricity based on price changes in the previous or later period, that is, long-term consumers. This section assumes that 5% of the electricity users participating in DR are short-term consumers and 5% are long-term consumers. Therefore, its demand-price elasticity matrix contains both self-elasticity and mutual-elasticity coefficients. The calculated total operating cost and the total user purchase cost are 724877$and 102099$, respectively. Compared with the case one result, the total operating cost is reduced by 4%, and the total user purchase cost is reduced by 10%.

Figs. 6 and 7 show the hourly load demand and start-stop cost change charts for Case 1 and Case 2, respectively.

Fig. 6 shows that compared with case 1, the load demand in the case 2 peak period decreases and increases in the low load period. This change rule is caused by the change in the real-time electricity price. For short-term users, the standard deviation and average peak load demand per hour decreased from 329.89 MW, 2476 MW–288.11 MW and 2365 MW, respectively, which represents 13% and 5% decrease. Considering both short-term and long-term users, the standard deviation and average peak load demand per hour decreased to 264.56 MW and 2301 MW, respectively, which means a 20% and 7% reduction. Because case 2 considers the interaction between real-time electricity price and DR, the optimal purchase price decreased from 23.4$/MWh to 21.3$/MWh, a 9% reduction. The above results show that DR can provide an effective peak load shifting effect in high wind permeability systems.

As shown in Fig. 7, the case two model can effectively reduce the start-up and shutdown costs of a thermal power unit compared with case one. Table 2 shows the detailed costs of Case 1, Case 2, Case 3 and Case 4. In Case 2, the cost of rotating the backup increased compared with Case 1. The reason is that considering the interaction between real-time electricity price and DR, power users can transfer peak loads to low and non-peak periods. At the same time, to avoid the insufficient interaction of power users in DR during the original peak period, the more rotational reserve is needed. The increased cost of rotating backup is much lower than the reduced cost of starting and stopping operations. Compared with case one, case two has a lower cost of the load-demand transfer, while case two has the lowest cost in short-term and long-term mixed situations. The reason is that the load demand curve of load demand transfer cost is closely related. The more stable the curve, the lower the cost. The above results show that DR can effectively reduce the total cost of the

Table 1
The real time price optimization results of case 2.

Time	Short term ($/MWh)	Short-term, long-term ($/MWh)	Time	Short term ($/MWh)	Short-term, long-term ($/MWh)
1	22.34	18.41	**13**	23.19	26.46
2	18.95	16.99	**14**	23.19	26.07
3	16.04	14.82	**15**	23.19	22.51
4	16.04	14.82	**16**	23.19	22.43
5	15.12	14.66	**17**	25.06	27.82
6	15.12	14.74	**18**	26.91	30.12
7	15.89	15.19	**19**	25.60	29.26
8	15.89	15.19	**20**	24.97	28.31
9	16.57	15.58	**21**	24.97	27.96
10	24.79	26.88	**22**	23.40	23.35
11	23.40	26.39	**23**	23.40	21.05
12	24.22	27.46	**24**	23.19	18.90

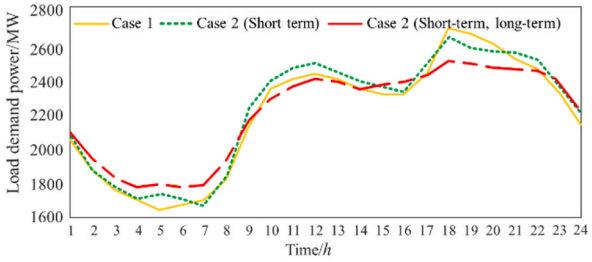

Fig. 6. The load demand of case 1 and case 2.

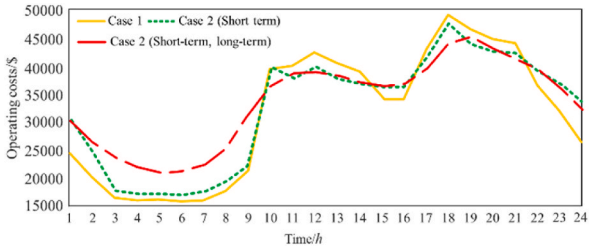

Fig. 7. The decision results of case 1 and case 2 operation cost.

Table 2
The detailed cost of case 1 case 2 case 3 and case 4.

	Operating cost, start-stop cost ($)	Spinning reserve cost ($)	Total cost of wind power ($)	Load demand transfer cost ($)
Case 1	497529	42608	208742	455
Case 2 (Short term)	488484	45788	210532	432
Case 2 (Short-term, long-term)	467053	49197	210221	406
Case 3	770952	67370	220878	98103
Case 4 (Short term)	748661	71525	233987	13039
Case 4 (Short-term, long-term)	672434	73027	231206	9831

system in a high wind penetration system.

5.3. *Case 3 simulation result analysis*

Case 3 is to SCUC decision-making under fixed electricity price scheme, considering wind power output uncertainty and power system component failure. The total operating cost obtained from the solution is 115703$. Compared with the case one result, the total operating cost increased to 407969$, or 54%. Detailed costs of Case 3 and Case 4 are shown in Table 2. The reason is that, considering the faults of power system components, operators have to dispatch power generating units with higher output, better performance and higher cost to meet the basic requirements of keeping power off after system failure. At the same time, in case three, full generating units usually start and stop operation at non-economic points under normal conditions, and in case of failure, wind turbines generate more power, load demand transfer is also increased, etc. These factors lead to increased costs.

5.4. *Case 4 simulation result analysis*

Case four considers the interaction between real-time electricity price and DR, and also considers the uncertainty of wind power output and power system component failure to make SCUC decision. Table 3 shows the real-time electricity price in Case 4.

Compared with Table 1, Table 3 has a large price fluctuation, indicating that the system adjusts prices more frequently in case of failures to meet the flexibility requirements of the power system.

As can be seen from Table 2, for short-term power consumers, the total operating cost from Case 4 solution is 106,7212$. The total operating cost was reduced by 7.7% compared with the case three results. For short-term and long-term hybrid power consumers, the total operating cost obtained by Case 4 is 986498$. The total operating cost is reduced by 15% compared with the case three results. As in case 2, the introduction of the interaction between real-time electricity price and DR can significantly reduce the operating costs of power systems.

Figs. 8 and 9 show the change of hourly load demand and operating start-stop costs for Case 3 and Case 4, respectively. From Figs. 8

Table 3
The real time price optimization results of case 4.

Time	Short term ($/MWh)	Short-term, long-term ($/MWh)	Time	Short term ($/MWh)	Short-term, long-term ($/MWh)
1	21.79	20.41	**13**	24.12	26.55
2	19.06	16.78	**14**	23.42	25.14
3	14.78	14.59	**15**	23.19	23.08
4	14.78	14.52	**16**	23.19	22.81
5	14.49	14.23	**17**	25.81	27.89
6	14.63	14.40	**18**	27.99	30.41
7	15.58	15.17	**19**	26.80	29.49
8	15.58	15.17	**20**	26.02	28.44
9	16.12	15.93	**21**	25.94	28.36
10	25.53	27.02	**22**	24.29	24.64
11	23.96	26.46	**23**	23.61	22.65
12	25.43	27.68	**24**	23.00	21.05
12	24.22	27.46	**24**	23.19	18.90

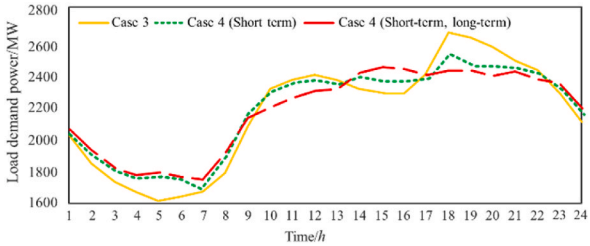

Fig. 8. The load demand of case 3 and case 4.

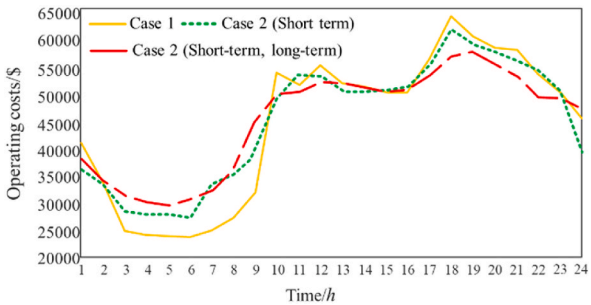

Fig. 9. The decision results of case 3 and case 4 operation cost.

and 9, we can see that the introduction of the interaction between real-time electricity price and DR can significantly improve the peak cutting and valley filling capacity, and effectively reduce the cost of the power system.

Table 2 shows the detailed costs of Case 3 and Case 4. The reason for the difference in cost size of each item is consistent with case two. The above results show that the higher the ratio of power users participating in DR, the smaller the impact of power system failure.

6. Conclusion

This paper presents a two-stage SCUC model considering uncertainty and DR to minimize operating costs. The model indirectly adjusts DR by optimizing the real-time pricing mechanism to improve the flexibility of the power system. The simulation and analysis results showed that the implementation of the DR strategy based on price incentive improves the flexibility level of the power system and reduces the operating cost of the power system. In addition, the DR composed of short-term and long-term mixed consumers can further reduce the operating costs of power systems. Furthermore, under the influence of uncertainties and system component faults, the power system's peak-load shifting capacity is enhanced by the stimulation of electricity price.

Declaration of competing interest

The author declare no conflict of interest.

References

[1] Fokui Willy Stephen Tounsi, Michael Saulo, Livingstone Ngoo, Controlled electric vehicle charging for reverse power flow correction in the distribution network with high photovoltaic penetration: case of an expanded IEEE 13 node test network, Heliyon 8 (3) (2022), e09058.
[2] M.A. Mohamed, A. Almalaq, H.M. Abdullah, K.A. Alnowibet, A.F. Alrasheedi, M.S.A. Zaindin, A distributed stochastic energy management framework based-fuzzy-PDMM for smart grids considering wind park and energy storage systems, IEEE Access 9 (2021) 46674–46685.
[3] H. Tan, W. Yan, Z. Ren, Q. Wang, M.A. Mohamed, A robust dispatch model for integrated electricity and heat networks considering price-based integrated demand response, Energy 239 (2022), 121875.
[4] M.N. Azimi, Z. Mohammad, P. Sanjeevikumar, et al., An efficient, robust optimization model for the unit commitment considering renewable uncertainty and pumped-storage hy-dropower[J], Comput. Electr. Eng. (2022) 100.
[5] Yan Sun, Yan Chen, M.O. Dong, et al., Joint chance constrained unit commitment with wind farms based on risk sharing[J], Power Syst. Technol. 46 (8) (2022) 2996–3007.
[6] Nanyang Zhang, Guojiang Xiong, Jinlong Chen, et al., Unit commitment of the power system containing wind power via quantum discrete differential evolution [J], Power System and Clean Energy 38 (1) (2022) 89–96.
[7] H. YingYi, DG. F G A, Uncertainty in unit commitment in power systems: a review of models, methods, and applica-tions[J], Energies (20) (2021) 14.
[8] Xingquan Ji, H.A.O. Qing, Yumin Zhang, et al., Unit commitment based on N-k distributionally robust optimiza-tion under uncertain distribution[J], Autom. Electr. Power Syst. 46 (2) (2022) 56–64.
[9] Nikoobakht Ahmad, Aghaei Jamshid, Mardaneh Mohammad, et al., Moving beyond the optimal transmission switching: stochastic linearised SCUC for the integration of wind power generation and equipment failures uncertainties[J], IET Generation, Transm. Distrib. 12 (15) (2018) 3780–3792.
[10] D. Jiménez, A. Angulo, A. Street, et al., A closed-loop data-driven optimization framework for the unit commitment problem: a Q-learning approach under real-time opera-tion[J], Appl. Energy (2023) 330.
[11] Y. Cho, T. Ishizaki, J.I. Imura, Three-stage robust unit commitment considering decreasing uncertainty in wind power forecasting, IEEE Trans. Ind. Inf. 18 (2) (2022) 796–806.
[12] Y. Wan, J. Qin, X. Yu, et al., Price-based residential demand response management in smart grids:A reinforcement learn-ing-based approach, IEEE/CAA J. Automatica Sinica 9 (1) (2022) 123–134.
[13] W. Fan, Z. Tan, F. Li, et al., A Two-Stage Optimal Scheduling Model of Integrated Energy System Based on CVaR Theory Implementing Integrated Demand response[J], Energy, 2023.
[14] L.I. Yuan-Zheng, N.I. Zhi-Xian, Jun-Tao Duan, et al., Demand response scheduling of major energy-consuming enterprises based on a high proportion of renewable energy power grid[J], Acta Autom. Sin. 49 (4) (2023) 754–768.
[15] Q. Ke, H. Qi, D. Yuefang, et al., Distributionally robust unit commitment with an adjustable uncertainty set and dynamic demand response, J. Energy (2023) 262.
[16] Yi Liang, P.A.N. Xiao, Xinyang Deng, et al., Operation optimization of electrothermal system combined with additional heat source and demand response[J], Power System and Clean Energy 36 (5) (2020) 90–96.
[17] Guodong Guo, Qianwen Xu, Yanfeng Gong, A distributed economic dispatching model for networked hybrid AC/DC microgrids considering demand response [J], Electrical Measurement & Instrumentation 60 (5) (2023) 116–125+153.
[18] L.I.U. Ren, L.I.U. Yang, Lixiong Xu, et al., multi-microgrid system collaborative optimization strategy considering dis-tributed demand response[J], Electric Power Construction 44 (5) (2023) 72–83.
[19] Bin Ding, Zhikun Xing, Fan Wang, et al., Collaborative optimal scheduling of integrated smart energy system con-sidering multi-load demand response[J], Journal of Global Energy Interconnection 5 (6) (2022) 583–592.
[20] J. Ma, B. Venkatesh, New real-time demand response market co-optimized with conventional energy market[J], IEEE Syst. J. (99) (2022) 1–12.
[21] Hongtao Huang, Ting Xu, Research on automatic mining algorithm of user information data based on SOM cluster-ing[J], Automation & Instrumentation 273 (7) (2022) 26–30.
[22] H.A. Aalami, M.P. Moghaddam, G.R. Yousefi, Evaluation of nonlinear models for time-based rates demand response programs[J], Int. J. Electr. Power Energy Syst. 65 (2015) 282–290.
[23] M. Ebeed, A. Alhejji, S. Kamel, et al., Solving the optimal reactive power dispatch using marine predators algorithm considering the uncertainties in load and wind-solar generation systems[J], Energies 13 (2020) 4316.
[24] Mostafa Rezaei, Udaya Dampage, Barun K. Das, Omaima Nasif, Piotr F. Borowski, Mohamed A. Mohamed, Investigating the impact of economic uncertainty on optimal sizing of grid-independent hybrid renewable energy systems, Processes 9 (8) (2021) 1468.
[25] Jian Chen, Khalid Alnowibet, Annuk Andres, Mohamed A. Mohamed, An effective distributed approach based machine learning for energy negotiation in networked microgrids, Energy Strategy Rev. 38 (2021), 100760.